Photodissociation of HI on the surface of large argon clusters: The orientation of the librational wavefunction and the scattering from the cluster cage.

Petr Slavíček, Pavel Jungwirth *

J. Heyrovský Institute of Physical Chemistry,

Academy of Sciences of the Czech Republic and Center

for Complex Molecular Systems and Biomolecules,

Dolejškova 3, 18223 Prague 8, Czech Republic

Marius Lewerenz

LADIR/Spectrochimie Moléculaire, UMR 7075, Bât F74, Bte 49,

Université Pierre et Marie Curie, F-75252 Paris Cedex 05, France

N. Hendrik Nahler, Michal Fárník, and Udo Buck

Max-Planck-Institut für Strömungsforschung,

Bunsenstrasse 10, 37073 Göttingen, Germany

(Dated: June 2, 2003)

* Author to whom correspondence should be addressed.
Electronic mail: pavel.jungwirth@jh-inst.cas.cz

Abstract

A new set of photodissociation experiments and simulations of HI on Ar_n clusters with an average size $\langle n \rangle = 139$ has been carried out for different laser polarizations. The doped clusters are prepared by a pick-up process. The hydrogen halide molecule is then photodissociated by a UV laser pulse and the outgoing H fragment is ionized by resonance enhanced multi-photon ionization (REMPI) in a (2+1)excitation scheme within the same laser pulse at a i wavelength of 243 nm. The measured time-of-flight spectra are transformed into hydrogen kinetic energy distributions. They exhibit a strong fraction of caged H atoms at zero kinetic energy and peaks at the unperturbed cage exit for both spin-orbit channels nearly independent of the polarization. At this dissociation wavelength the bare HI molecule exhibits a strict state separation, with a parallel transition to the spin orbit excited state and perpendicular transitions to the ground state. The experimental results have been reproduced using molecular simulation techniques. Classical molecular dynamics was used to estimate the HI dopant distribution after the pick-up procedure. Subsequently, quasi-classical molecular dynamics (Wigner trajectories approach) has been applied for the photodissociation dynamics. The following main results have been obtained. (i) The HI dopant lands on the surface of the argon cluster during the pick-up process, (ii) zero point energy plays a dominant role for the hydrogen orientation in the ground state of HI-Ar_n surface clusters, qualitatively changing the result of the photodissociation experiment upon increasing the number of argon atoms, and, finally, (iii) the scattering of hydrogen atoms from the cage which originate from different dissociation states seriously affects the experimentally measured kinetic energy distributions.

I. INTRODUCTION

Photodissociation of small molecules in different cluster environments has attracted much interest in recent years. Due to their finite size, the theoretical study of clusters is noticeably simplified compared to the complete treatment of bulk condensed matter. Moreover, various properties can be investigated as function of the cluster size.[1] In addition, some of these calculated quantities are now experimentally available so that a direct comparison is feasible.[2] Hydrogen halide molecules interacting with different rare gas clusters have served as prototype systems for such investigations using various theoretical approaches.[3–18] The reason is the very rich coupling behavior of the different electronically excited states that lead asymptotically to the ground and excited spin-orbit states. Depending on the magnitude of this coupling the excitation mechanism changes significantly when going from HCl to HI.[19–21] While for HCl, the ground and excited states are only reached by perpendicular transitions, HI exhibits a strict separation with a parallel transition to the excited and perpendicular transitions to the ground spin-orbit state. The HBr molecule is an intermediate case which behaves either way depending on the excitation wavelength. The behavior of the HI molecule has very recently been thoroughly investigated by a comprehensive analysis of all absorption coefficient and branching ratio data for the UV photodissociation using exact quantum simulations.[21] The results for the interaction potentials and the absorption coefficient are displayed in Fig. 1. There are mainly three potential curves involved, the $^1\Pi_1$ and the $^3\Pi_1$ states which are excited in a perpendicular transition and which lead to the ground spin-orbit state $I(^2P_{3/2})$, and the $^3\Pi_{0+}$ state which is reached in a parallel transition and leads to the excited spin-orbit state $I^*(^2P_{1/2})$. The characteristic feature of HI is that, over a large range of excitation wavelengths, all three potentials contribute to the final result. The analysis showed that there was no need to invoke coupling in the final state wave functions to explain the data. Thus, at a wavelength of 243 nm, the branching ratio $R = [I^*]/[I]$ is about one, which means that parallel (into the $^3\Pi_{0+}$ state) and perpendicular transitions (into the $^1\Pi_1$ and the $^3\Pi_1$ states) occur with roughly equal probabilities.

Now, the question arises how this complex behavior influences the photodissociation of HI on rare gas clusters. While most of the theoretical studies were carried out for the HCl-Ar_n system[5–7,10], the most detailed experimental results were obtained for HBr-Ar_n.[10,11] In a combined effort, experiments and calculations were directly compared and most of the behavior of HBr could be clarified, both for the interior and the surface position.[11,22] The photodissociation of HI placed on the surface of large neon, argon, krypton and xenon clusters was also measured in an additional experiment.[23] The gross features turned out to be quite similar to those obtained for HBr with a dominating cage effect. This general result is not straightforward, if we consider the behavior of the heterogeneous dimers. Namely in the ground state of all HBr-Rg and the HI-Ne complexes the H atom points into the direction of the rare gas atom, while this is not the case for HI-Ar. Here the I atom points to the Ar atom, therefore, during dissociation, the H atom is not hindered at all.[12,24,25] In a detailed calculation we have found that this trend of the dimer continues to HI-Ar_2, but is reversed for larger clusters.[12] There is a trade-off between induction forces that favor the I-H-Ar configuration and increasing dispersion forces that prefer the H-I-Ar configuration, moreover quantum delocalization of the librating hydrogen comes into play. Accurate quantum calculations of the librational wave functions demonstrate that for HI-Ar_3 the H atom points for the first time into the direction of the argon atoms. The flip back for HI-Ar_4 is shown to be an artefact of the reduced dimensionality of the vibrational calculations in the previous work.[12] Clusters from HI-Ar_5 onwards have hydrogen pointing towards the argons, in complete agreement with our experimental result.

In detail, the measured quantity, i.e., the kinetic energy of the outgoing H atom, appeared to be different from the results obtained for HBr. One of the reasons could be a different surface position of HI compared to HBr, because of the stronger interaction with the rare gas atoms. The other possibility is the complex coupling behavior mentioned earlier. In order to test these different hypotheses, we have carried out new experiments of the photodissociation of HI on the surface of Ar_n clusters for parallel and perpendicular polarizations. These experiments are compared with calculations of the dissociation dynamics for all three potential surfaces involved. It turned out that the scattering of the outgoing H atoms from the cluster played a major role in the interpretation of the data. In addition, also the exact position of the HI molecule on the surface of the Ar_n cluster was simulated by Molecular Dynamics (MD) simulations of the pick-up process.

II. EXPERIMENT

In the experiments the HI doped argon clusters are generated in a molecular beam apparatus. The HI molecules are photodissociated by UV light derived from a pulsed ns laser system. Within the same laser pulse the H atoms are ionized via a (2+1)REMPI (resonance enhanced multi-photon ionization) scheme and are energy-sensitively detected in a Wiley-McLaren time-of-flight mass spectrometer (WM-TOFMS) operated in the so called low-field mode. Details of this experimental setup have been described elsewhere.[26,27] Here only a short summary of the major components and of the various techniques of cluster preparation is given, including the implemented experimental improvements.[10,28]

To prepare the HI molecules in the surface region of the Ar_n cluster, the cluster beam is first produced by a supersonic expansion of pure Ar through a nozzle with conical shape with a diameter of 60 μm, an opening angle of 30° and a length of 2 mm. The measurements are carried out at an expansion pressure of 3.8 bar and a nozzle temperature of 216 K. According to the relation provided by Hagena[29] the average size of the Ar_n host clusters formed under these conditions is $\langle n \rangle = 139$. For the comparison with calculations, usually carried out for a single cluster size, the width of the cluster distribution should be taken into account. The FWHM of the log-normal distribution is in the order of the average cluster size.[30] Between the second and third chamber, which are both differentially pumped, the cluster beam passes through a scattering cell filled with HI molecules at a partial pressure of $4 \cdot 10^{-2}$ mbar. In the pick-up process under these conditions, it is most probable that only one HI molecule is adsorbed by the Ar_n cluster.[10]

Following cluster preparation the cluster beam enters the chamber containing the two-stage Wiley-McLaren type TOFMS.[31] To suppress the H atom background from hydrocarbons, the WM-TOFMS is surrounded by a copper shield mounted on a high-pressure helium compressor which results in a vacuum background pressure of $6 \cdot 10^{-9}$ mbar. In order to dissociate the clusters, the polarized laser light is focused into the WM-TOFMS by a lens with a focal length of 400 mm. The H atoms from the dissociation process are ionized in the same laser pulse using one-color (2+1)REMPI. The 243.06 nm light is generated by mixing the fundamental of a Nd:YAG laser (Quanta Ray GCR-5) with the frequency doubled output of a dye laser (LAS LDL 20505) operating at 630.15 nm and pumped by the second harmonic of the Nd:YAG laser at 532 nm. A schematic view of the experimental arrangement is given in the left part of Fig. 2. At their interaction point, the cluster beam, the dissociation laser, and the WM-TOFMS collection axis (detector axis) are oriented mutually perpendicular to each other. Thus, Doppler effects are eliminated in the photodissociation measurements. In the present experiments the laser is linearly polarized either in the plane formed by the laser and the cluster beam and at 90° to the detector axis (middle part of Fig. 2) or in the plane formed by the laser beam and the detector axis (right part of Fig. 2). Therewith in the latter case the laser polarization is parallel to the detector axis.

We first focus on the photodissociation process of free HI molecules. At a laser wavelength of 243 nm three repulsive states are involved which are populated by parallel and perpendicular transitions. For further details we refer to Fig. 1 and Ref. 21. In a molecular beam the HI molecules are available in all possible orientations. A high dissociation probability requires good overlap between the laser polarization and the transition dipole moment. The middle and left parts of Fig. 2 give a pictorial representation of the two laser polarizations, both for a parallel transition dipole moment as well as for the perpendicular case. Even though both kinds of states are populated, only the fragments from molecules with their molecular axis aligned parallel to the detector axis can be collected onto the detector. The other fragments miss the detector. This is a consequence of the operation of the WM-TOFMS in the so-called low-field mode where fragments with a velocity component perpendicular to the detector axis are not registered. The ions are extracted into the WM-TOFMS by a small electric field of 4 V. This causes a splitting of the peaks which originate from ions which are directly ejected toward the detector and others with an initial velocity in the opposite direction; then the latter ions are decelerated in the extraction field and their velocities are reversed. In this way we are able to detect slow fragments, even those with initially zero kinetic energy, which give rise to a signal between the peaks of the fast ions.

Fig. 3 shows a representative H fragment TOF spectrum from the photodissociation of pure HI molecules generated by the co-expansion of 8% HI seeded in Ar at room temperature. The outer peaks originate from the photodissociation of HI with the iodine partner fragment in its spin-orbit ground state. The inner peaks correspond to H fragments with a partner fragment I*. These H atoms appear later in the forward part because of their lower kinetic energy corresponding to the higher internal energy of the iodine atom. If their trajectories point initially away from the detector their lower kinetic energy causes them to be slowed down more easily, which results in an earlier appearance in the rear part of the spectrum. In Fig. 3 the measurement is represented by circles. The solid line corresponds to a fit carried out by our Monte-Carlo particle trajectory simulation program[32] which takes into account the photodissociation process with its angular distribution, the velocity of the cluster beam, the finite interaction volume, the detector dimensions, the different electric deflection fields, and the electronic response function of the detector. For this fit we use values for the anisotropy parameter of the angular distribution β and the branching ratio R from the recent publication of Le Roy and coworkers[21] ($\beta(\mathrm{I}) = -1.00$, $\beta(\mathrm{I}^*) = 2.00$, $R = 0.934$). The excellent agreement between fit and measurement proves the reliability of our data and the data evaluation procedure. The outer peaks have less intensity because of a lower detection efficiency for higher energy particles due to their higher transverse velocity.[10] We note that none of the molecules with the "wrong" orientation reaches the detector.

When the dissociation process takes place in a cluster environment the H fragment trajectories are influenced by the cluster cage. Our measured time-of-flight spectra can be transformed into H atom kinetic energy distributions using a least-square fit method with the above mentioned program. The various contributions which can be derived from the measured kinetic energy of the H atom, $E_{kin}(\mathrm{H})$, are best discussed in terms of the energy balance of the photodissociation

$$h\nu + E_{int}(\mathrm{HI}) = D_0 + E_{int}(\mathrm{I}) + E_{kin}(\mathrm{H}) + E_{clu} \tag{1}$$

where the laser excitation energy $h\nu$ and the dissociation energy D_0 of HI (3.055 eV)[33] are known, and $E_{kin}(\mathrm{H})$ is measured. The kinetic energy of the I fragment is known from momentum conservation. The excitation of the upper spin-orbit state (I^*) of the I product channel is allowed for by the term $E_{int}(\mathrm{I})$ and is measured as kinetic energy loss of the H atom. The influence of the cluster is expressed by the continuous energy loss E_{clu} of the H atoms caused by collisions and capture processes within the Ar cage. This leads to delayed exit or perfect caging, depending on the position of the HI molecule in the cluster environment and the initial direction of the H atom recoil. Both the co-expansion and the pick-up process create HI molecules which are mainly in their ground rotational and vibrational state which implies $E_{int}(\mathrm{HI}) = 0$.

In addition to the kinetic energy of the H fragment also the directions of the trajectories are influenced by collisions and scattering processes involving the cluster cage. Both processes induce a change in the angular distribution of the fragments which can range from a slight change to a total loss of information about the initial angular distribution. The way scattering processes affect the photodissociation of diatomic molecules on the surface of a cluster is sketched in two dimensions in Fig. 4 which shows HI molecules (I: white circle, H: black circle) on the surface of the Ar cluster with three icosahedral shells represented by concentric rings. The double-headed-arrows again indicate the transition dipole moment. The H fragment from the dissociation of the molecule in the left part would reach the detector with a probability of one in the case of a free molecule. The H atom in the right part would leave the WM-TOFMS without arriving at the detector. The presence of the Ar cluster scrambles the trajectories such that some fragments are scattered away from the detector in the left part (dashed lines) or scattered into the detector in the right part (solid lines). For a measured kinetic energy distribution of the H atom with a laser polarization of 90°, like in the figure, the signal from perpendicular transitions leading to H + I will decrease and a contribution from parallel transitions leading to H + I* will appear. Both channels will become more isotropic.

Fig. 5 gives a three-dimensional view of this effect. The big ball depicts the Ar cluster, the small ball pairs represent the HI molecule, the big double-headed-arrows the laser polarization, and the small ones the transition dipole moment. All shown molecules are photodissociated with the same probability according to the identical overlap between the laser field $\vec{E_L}$ and the transition moment $\vec{\mu}$. The left part can be a model for nearly total loss of the information about the initial angular distributions. Usually only the molecules sitting on the poles would contribute to the distribution due to scattering by 0° or 180°. But the scattering processes weaken the signal from the pole molecules and allow the detection of fragments from equatorial molecules. The H fragments detected from the right part of the figure are distributed in a perfectly isotropic fashion because of their symmetric geometry around the detector axis and the identical overlap between $\vec{E_L}$ and $\vec{\mu}$. Their only contribution originates from a scattering by an angle around 90°. A mathematical description of the scattering process and its influence on the angular distribution is given in Sec. IV E.

III. EXPERIMENTAL RESULTS

We have carried out measurements for two polarization angles of the laser light at 0° and 90° with respect to the detector axis. The results are depicted in Fig. 6 as black points. Both curves are characterized by three peaks. The peak at zero kinetic energy which corresponds to completely slowed down H atoms is always the largest one. Two other peaks appear near 1.0 eV and 2.0 eV and correspond to H atoms which have left the argon cage without loosing energy. The peak at 2.0 eV represents production of ground spin-orbit state H+I, while the one at 1.0 eV correlates with the excited spin orbit state H+I*. According to the experimental result for the monomer and the theoretical prediction, the latter peak is expected at 0° polarization and the former one at 90° polarization as was demonstrated in Fig. 3 and Fig. 1.

The experimental result for the photodissociation of HI on argon clusters is clearly completely different. At 0° polarization, we observe a substantial contribution from the ground state around 2.0 eV, while at 90° polarization the intensity caused by the excited state close to 1.0 eV cannot be overlooked. A preliminary analysis of the anisotropy factor gives $\beta = 0.0 \pm 0.1$ for the ground state and $\beta^* = 0.3 \pm 0.2$ for the excited state, while these values are $\beta = -1.0$ and $\beta^* = 2.0$ for the isolated molecule, respectively. Thus the interaction with the cluster causes the loss of the strong anisotropy in the dissociation of the bare molecule. We note, however, that the branching ratio in the cluster $R = 0.85 \pm 0.1$ is about the same as for the bare HI molecule ($R = 0.934$).

IV. THEORETICAL METHODS

A. System and potentials

We have simulated clusters containing three argon layers with a hydrogen iodide impurity attached to the cluster. For the photodissociation dynamics we have adopted an icosahedral structure with 147 atoms, while for the pick-up simulations we have assumed slightly smaller clusters with lower symmetry. The potential energy surface of the HI-$(\mathrm{Ar})_n$ cluster in the ground state was modeled as a sum of a three body potential for the HI-Ar interaction[34] and by pair potentials for the remaining interactions. For the argon-argon interaction we have adopted the potential of Aziz and Slaman.[35] The bonding interaction between hydrogen and iodine is approximated by a harmonic potential.[36]

This potential energy surface has been used for the calculation of the ground state vibrational wavefunction of the system. For the pick-up simulations, however, this potential surface cannot be used directly. This is due to the fact that the diagonalization of the vibrational/librational wavefunction in every step of the MD simulation is computationally infeasible for 50 ns simulations. Therefore we have substituted the three body HI-Ar potential by an effective two body isotropic potential. This potential has been obtained by averaging over all possible HI orientations. In this way, the potential energy surface for pick-up simulations becomes pairwise additive. This effective HI-argon potential has been fitted to a standard Lennard-Jones form:

$$V_{LJ} = 4\epsilon \left(\left(\frac{\sigma}{r}\right)^{12} - \left(\frac{\sigma}{r}\right)^{6} \right), \tag{2}$$

with $\sigma = 3.71$ Å and $\epsilon = 134.1$ cm^{-1}.[22] This effective potential correctly describes the interactions of the HI dopant embedded in the cluster, where the hydrogen librational wavefunction is truly isotropic. The interaction of a surface dopant with the cluster is, however, slightly underestimated since the hydrogen wavefunction is no more isotropic, but is preferentially oriented towards the argon clusters.

For the argon-argon interaction we have chosen two model potentials for the pick-up simulations. The first one is a standard Lennard-Jones potential with $\sigma = 3.405$ Å and $\epsilon = 83.3$ cm^{-1}.[37] The second model is the more accurate HFD-B potential of Aziz and Slaman[35], identical with the one used for the simulation of the photodissociation dynamics. The well depth of the latter potential is almost 100 cm^{-1}, therefore, Aziz-Slaman argon clusters are stiffer than the standard Lennard-Jones argon clusters. Since this Lennard-Jones potential is still used in many applications, we discuss the influence of the potentials in detail in Sec. IV.

For low-lying excited electronic states of HI, the potential is constructed using a Diatomics-in-Molecule (DIM) Hamiltonian. In this approach, the anisotropy of the iodine-argon interaction is explicitely taken into account. The repulsive hydrogen-argon interaction, the slope of which strongly influences the strength of caging, is taken from accurate *ab initio* calculations.[7] For Ar-Ar the potential of Aziz and Slaman was used.[35] DIM components for the argon-iodine interaction were taken from Ref. 38. Three electronic states are particularly populated during the HI photodissociation following a 243 nm laser pulse excitation: $^1\Pi_1, ^3\Pi_{0+}$, and $^3\Pi_1$. These potentials have been modeled as single exponentials.[39] For the electronically excited potential energy surfaces the same argon-argon potential as for the ground state has been used.

B. Pick-up simulations

Co-expansion and the pick-up technique for the preparation of mixed clusters are generally expected to lead to different cluster isomers: structures with an embedded impurity in the former case and a surface embedding isomer for the latter case. Since the clusters have enough time for equilibration prior to photodissociation, this assumption implies that the system is non-ergodic, i.e., that the clusters are solid after their preparation. It is challenging to simulate the pick-up process to check the validity of the basic assumption that the chromophore stays in the surface of the cluster. It has been shown recently[40] that the actual result of the pick-up process depends on the particular system, cluster temperature, buffer gas temperature, and cluster beam velocity. In this study we address the question where the HI chromophore does land during the pick-up process on argon clusters. Does HI stay on the surface or does it penetrate deeper into the cluster? And, if it remains on the surface, does it occupy a substitutional or an adsorbed position?

Molecular dynamics is a suitable tool to provide an answer for these questions. Note at this point that it is imperative to use a dynamical method for the modeling of the pick-up process, even though the system is finally to a large extent equilibrated. The reasons are that we do not know the target temperature of the system in advance and we want to describe states which are possibly only kinetically (and not necessarily thermodynamically) stable, due to the lack of ergodicity in the system. The simulation of the pick-up process indicates the dopant position, and it also represents an important test of the quality of the employed ground state potentials.

We have used a standard Verlet algorithm for the integration of Newton's equations of motion.[41] The time step was set to 10 fs, which is a reasonable choice for this type of systems.[40] Initially, clusters are prepared at $T = 27$ K. In each case, equilibration is performed for 10 ns. The cluster is then randomly rotated and the dopant is sent towards the equilibrated cluster with a random impact parameter. Impact velocities are sampled according to the distribution resulting from the HI temperature of 300 K and the cluster beam velocity of 450 ms^{-1}. Each of the pick-up simulations was run for 50 ns. It has been shown by Vach[40] and confirmed here that an order of magnitude longer simulations do not change the results significantly. All quantities were recorded every 100 time steps. In total, 200 trajectories have been collected. For the determination of the final position, we have recorded the dopant distance from the cluster center of mass. We have then calculated the radial density of dopant atoms $\rho(r_{com})$ as a function of the distance from the cluster center of mass. Alternatively, we have recorded the number of nearest neighbors of the dopant atoms at its final position. We define the nearest neighbor as an argon atom which is closer than 4.3 Å. The corresponding density function is denoted as $\rho(n)$.

In order to describe the experimental situation in the pick-up simulation we have chosen Ar_{130} as the initial cluster size. This system is an incomplete three layer cluster, which falls within the range of the experimental cluster size distribution. For the photodissociation dynamics, we assume that the cluster has an icosahedral symmetry, which corresponds to Ar_{147} for a three layer Lennard-Jones system. This is also a system of exceptional stability (magic number cluster). For the pick-up simulation we have chosen to use the slightly smaller and less symmetric cluster, in order to increase isomerization rates. We have also generated a limited number of pick-up trajectories with different cluster sizes including the compact Ar_{147} system. The distribution functions were qualitatively the same, but the time required to achieve convergence was somewhat larger for Ar_{147}.

C. Initial state

By pick-up simulations we have determined positions within the cluster which are occupied by the dopant under experimental conditions. For these positions, we have performed structure optimizations and, simultaneously, we have calculated the initial vibrational wavefunction.

Similarly to our previous studies[7,9,11,12] we have used a partially separable approach, in which the total vibrational wavefunction is expressed as:

$$\Psi(\rho, q_1, q_2, ..., q_{3n-6}, \Theta, \Phi) = \frac{\chi(\rho)}{\rho}\phi_1(q_1)....\phi_{3n-6}(q_{3n-6})\phi_{lib}(\Theta, \Phi, \{q_i\}) \quad (3)$$

where q_i are the normal coordinates of the heavy atom cage and ρ is the H-I separation. The factor $1/\rho$ originates from the use of spherical coordinates. The cage modes are taken into account within the harmonic approximation, while the librational wavefunction of the HI molecule $\phi_{lib}(\Theta, \Phi, \{q_i\})$, which parametrically depends on the cage coordinates, is calculated by diagonalization of the rotational Hamiltonian appropriate for HI

$$\hat{H} = \frac{\hat{j}^2}{2\mu_2 r^2} + V(\Theta, \Phi, \{q_i\}) \tag{4}$$

in the basis of spherical harmonics. Here, μ is the reduced mass of the HI molecule and $V(\Theta, \Phi, \{q_i\})$ is the full potential energy surface of the system. This approximation is essentially an adiabatic separation of the fast HX librational motion and slow motions of the heavy cluster particles. We have then optimized the heavy particle positions by minimization of the lowest eigenvalue of this Hamiltonian. The final librational wavefunction is thus obtained by a repeated diagonalization in the basis of spherical harmonics for the optimal cluster geometry.

Nowadays, it is technically possible to obtain the fully coupled wave function of the vibrational ground state even for extended molecular clusters. Due to its favorable scaling with system size, the Diffusion Monte Carlo (DMC) method can be used for this purpose.[42] The DMC method exploits the isomorphism between the time-dependent Schrödinger equation expressed in terms of imaginary time and a multidimensional diffusion equation. The principles of the DMC method and some important algorithmic strategies are described in detail elsewhere.[43,44] The present implementation, which is based on that described in Refs. 45,46, uses weighted random walkers and stochastic branching and termination.

It is appealing to use the DMC method to sample initial conditions for molecular dynamics simulations. However, the DMC method produces a swarm of random walkers, which sample the wavefunction rather than its square (i.e., probability) and special techniques have to be used to find the proper quantum density. To perform a Wigner transformation within the frame of the DMC method is even more complicated.[47] We have used DMC as a benchmark method to re-investigate the structure of HI-Ar_n ($n = 1 - 6$) systems and to test the applicability of the reduced dimensionality description outlined above and also used in our previous study.[12]

D. Photodissociation simulations

For the simulations of the photodissociation dynamics we have employed the method of Wigner trajectories. Within this approach, the quantum nature of the initial state is taken into account, while the dynamics following the photoexcitation is modeled classically. This approach is well justified in the present situation. The initial state is strongly quantum mechanical, with large amplitude delocalized motions at least in several degrees of freedom. On the other hand, after photoexcitation the importance of quantum effects is significantly reduced, since several electronvolts of excess energy have been pumped into the system. In the Wigner trajectories method, initial positions and momenta for a set of trajectories are determined by a Wigner transform of the initial wavefunction.[48] The direct use of this set of coordinates and momenta as initial conditions for a classical MD simulation of photodissociation corresponds to a vertical excitation by an infinitely short pulse. However, in the experiment a laser source with a fixed wavelength is employed. Therefore we have to filter the initial conditions in such a way that the following energy relation is satisfied:

$$\hbar\omega = E^{e}_{Ar-HI} - E^{g}_{Ar-HI}, \tag{5}$$

where $\hbar\omega$ is the photon energy, and E^{g}_{Ar-HI} and E^{e}_{Ar-HI} are the interaction energies between argons and HI in the ground and in the excited states. In practice, we first sample the librational and cage parts of the wavefunction and then we simply extend the H–I distance such that the above energy relation is fulfilled. This procedure is well justified since for the present system and laser wavelength of 243 nm, the energy depends almost exclusively on the H–I distance and not on the librational motion or (small) cage displacements.

Three electronic states of HI are involved in the photodissociation process at 243 nm: $^1\Pi_1$ and $^3\Pi_1$ leading to the lower spin-orbit H+I asymptote, and the $^1\Pi_{0+}$ state correlating with the upper spin-orbit channel H+I*. The branching fraction Γ defined as

$$\Gamma = \frac{[\mathrm{I}^*]}{[\mathrm{I}] + [\mathrm{I}^*]} \tag{6}$$

is approximately 0.5 for the 243 nm photoexcitation.[21,49] Note at this point that non-adiabatic couplings between the three excited states in the gas phase are negligible. We have performed photodissociation simulations on all three potential energy surfaces, corresponding to different HI electronic states. Observables have then been weighted by the branching fraction (the ratio between the $^1\Pi_1$ and $^3\Pi_1$ states, both correlating with the spin-orbit ground state, has been set to 1:1.6[21,49]; the results are, however, insensitive to the exact value). We have assumed that the branching fraction is not significantly affected by the argon cluster environment. For each state, we have collected 30000 trajectories. This large number of trajectories is required to obtain well converged kinetic energy distributions as functions of both energy and scattering angle. The simulation time for each trajectory has been 1.5 ps with a time step of 0.0241 fs. A standard Gear predictor-corrector algorithm has been used for the integration of the classical equations of motion.

E. Protocol for simulations of photodissociation using polarized light

First we introduce the employed coordinate systems. The HI molecular axis is described by a vector $\vec{r}_{HI}$. If we take a vector $\vec{E}$ as a reference axis we can introduce polar coordinates Θ_E and ϕ_E. In a similar fashion, we can set the detector axis $\vec{D}$ as a reference vector, leading then to polar coordinate Θ_D and ϕ_D. The photodissociation experiment is performed with a polarized laser beam. HI molecules are promoted to the $^1\Pi_1$ and $^3\Pi_1$ states (corresponding to the ground state asymptote) via a perpendicular transition, and to the $^1\Pi_0$ state via a parallel transition. For a bare hydrogen halide molecule a kinetic energy distribution corresponding to only one of the states is then recorded for each polarization (see Fig. 2). The situation is more complicated for the photodissociation in the cluster since scattering of the dissociating hydrogen comes into play as outlined in Sec. III.

As a result of molecular dynamics simulations we obtain kinetic energy distributions for the outgoing hydrogen corresponding to different states $P_{^1\Pi_1}(E), P_{^3\Pi_1}(E)$, and $P_{^1\Pi_0}(E)$. Let us introduce hydrogen kinetic energy distributions corresponding to the excited $P_e(E)$ and ground $P_g(E)$ dissociative asymptotes. $P_e(E)$ is equivalent to $P_{^1\Pi_0}(E)$, while $P_g(E)$ is obtained as a sum of $P_{^1\Pi_1}(E)$ and $P_{^3\Pi_1}(E)$. We can also collect the angular information from the simulations. The probability of finding the hydrogen fragment with a kinetic energy E scattered at an angle Θ_S is $P_g(E, \Theta_S)$ and $P_e(E, \Theta_S)$ for the ground and excited spin-orbit states, respectively. Here, we take the molecular axis at time $t = 0$ as a reference axis. Note at this point that the distributions $P_g(E, \Theta_S)$ and $P_e(E, \Theta_S)$ are normalized in spherical coordinates (i.e., the total hydrogen population is divided by a factor $\sin \Theta$).

A molecular cluster is randomly oriented in space. If the system is subjected to polarized light, clusters with the HI molecule oriented parallel or antiparallel to the electric field are transferred to the spin-orbit excited channel, while clusters with the HI molecule perpendicular to the electrical field are promoted to the ground spin-orbit dissociative channel. More precisely, the probability of exciting the HI molecule into the H+I channel is proportional to $\sin^2(\Theta_E)$, while the probability of excitation into the H+I* channel is given by the factor $\cos^2(\Theta_E)$. The branching fraction *Gamma* defined previously is taken from the experiment.[21,49] The population P of hydrogen atoms reaching the detector with a kinetic energy E is then given by the integral:

$$\begin{aligned} P(E) = \frac{1}{2}(1-\Gamma) \int_0^{2\pi} \int_0^{\pi} \sin\Theta_E P_g(\Theta_D, E) \sin^2(\Theta_E) d\Theta_E d\phi_E \\ +\Gamma \int_0^{2\pi} \int_0^{\pi} \sin\Theta_E P_e(\Theta_D, E) \cos^2(\Theta_E) d\Theta_E d\phi_E \end{aligned} \quad (7)$$

where the angle Θ_D in case of a parallel arrangement of the experiment coincides with Θ_E. The factor $\frac{1}{2}$ is introduced because of different normalizations of $\sin^2\Theta$ and $\cos^2\Theta$ when integrated over a sphere. Note at this point that we assume a delta function detector. This is an acceptable approximation since the experimental detector has an opening angle of only 2°. Numerically, the distribution functions $P_g(E, \Theta_S)$ and $P_e(E, \Theta_S)$ are constructed by collecting the hydrogen population with a given E and Θ_S in 50 bins. Thus, the angular resolution in the MD simulation is 3.6^o.

V. THEORETICAL RESULTS

A. Pick-up simulation

We have investigated the pick-up process for clusters containing initially 130 argon atoms. The potential model used for the argon-argon interaction turns out to be critical for the result of the pick-up simulation. Therefore, we discuss separately the simulations with the two different Ar-Ar potentials introduced in Sec. III.

Figure 7a shows the density of the HI molecule as a function of the dopant distance from the cluster center of mass for the Lennard-Jones interaction potential. For comparison, the density for the argon atoms is also displayed. In the argon density curve we can identify four distinct peaks representing the central atom, first, second, and third icosahedral layer.

The cluster is solid under experimental conditions.[50] After the collision with the dopant the cluster reorganizes to a certain extent. The isomerization rate is high before the cluster cools down again by evaporation of argon atoms. Fig. 7a indicates clearly that the HI dopant prefers a position in the second layer, which is almost fully embedded in the cluster. Some 55 % of HI dopants, however, stay on the surface of the cluster, but this number rapidly decreases with increasing temperature. Another way to visualize the final dopant position is to display the number of argon atoms which are in direct contact with the dopant molecule. This graph is depicted in Fig. 7b, where we can distinguish fully solvated chromophores ($n_{close} \approx 12$) from chromophores solvated in the surface ($n_{close} \approx 6$), and chromophores which occupy the smooth adsorption site ($n_{close} \approx 3$). Figure 7b gives the same qualitative picture of the process as Fig. 7a, namely that the dopant molecule stays in the second and outermost layers. It typically takes several nanoseconds before the dopant lands in the final position. We can conclude that for a Lennard-Jones potential the outer shell behaves like a liquid, while the second shell has a semi-liquid character with argon atoms remaining most of the time in their equilibrium position, with infrequent isomerizations. Finally, the inner shell is not accessible to the dopant.

A rather different picture emerges from a simulation using the more accurate Aziz-Slaman argon-argon interaction potential (see Fig. 8). Dopant molecules stay in the surface, and virtually no HI penetrates into the cluster. Most of the dopants occupy substitutional positions, interacting with approximately 6 to 8 argon atoms. Only a minor fraction lands on the surface, at smooth adsorption sites which is displayed in Fig. 8b. The argon cluster is more solid for the HFD-B potential, the argon atoms are closer to each other than in the case of the standard Lennard-Jones potential, and the impurity has only a small chance to penetrate into the cluster.

There is a clear disagreement between results obtained using the standard Lennard-Jones potential and the HFD-B potential. The HFD-B potential is definitely the more reliable interaction potential. The Lennard-Jones potential and its parameterization was originally derived from bulk measurements of the second virial coefficient[51] and gave also good agreement with experimental data on liquid and solid properties. Later on it was recognized that, based on new experimental data, the attractive part was in error.[52] In contrast, the HFD-B potential reproduces the best available scattering, spectroscopy, transport, and other gas phase data and is considered as genuine 2-body potential.[35] Possible quantum effects can be estimated by calculating the Gaussian Feynman-Hibbs effective quantum potential[53] given by the equation:

$$V_{GFH}(|\mathbf{r}|) = \left(\frac{6\mu}{\pi\beta\hbar^2}\right)\int_{\infty}^{-\infty}\int_{\infty}^{-\infty}\int_{\infty}^{-\infty} V_C(|\mathbf{r}+\mathbf{u}|)\exp\left(-\frac{6\mu}{\beta\hbar^2}\right)\mathbf{u}^2 d\mathbf{u} \tag{8}$$

where V_C is the interaction potential, μ is the reduced mass and $\beta = 1/kT$. Evaluation of the above integral for the HFD-B potential at $T = 27$ K gives a well depth which is only 2 cm^{-1} smaller than for the classical potential. The result of the pick-up simulation is stable with respect to such a small change. We observe the solid-liquid "phase transition" only for well depths around 85 cm^{-1}. For the Aziz-Slaman potential the results are also stable with respect to a change of the initial cluster temperature by several Kelvins.

B. Optimized initial structure on the surface and in the second shell

The results of the simulations described in the previous section have been used as an indication where the HI molecule lands during the pick up process. The actual photodissociation simulations are done under the assumption of zero cluster temperature before HI excitation. Since the final dopant site is different for the two widely used argon-argon interaction potentials, we have decided to study separately the photodissociation process for the HI dopant placed either into the surface or in the second solvation shell of a three-layer argon cluster. The surface position corresponds to the more reliable Aziz potential, while the use of the Lennard-Jones potential leads to large HI abundance in the second shell. It is well known that argon clusters prefer the icosahedral arrangement up to at least 750 argon atoms.[50] Therefore, we have adopted an icosahedral three-layer structure for the Ar_{147} cluster. However, it should be mentioned that argon clusters prepared experimentally by supersonic jet expansion have a certain distribution in sizes and shapes, and that the rapid cooling process can lead to a non-negligible population of energetically higher isomers in the cluster beam.

The dopant cluster was prepared by replacing one argon atom either in the outer or second shell by a single HI dopant. A question arises whether one has to take into account also the smooth adsorption site, i.e., HI placed on the surface of an argon cluster rather than substituting an argon atom from the surface layer. The pick-up simulations indicate that the substitutional positions dominate strongly for all tested potentials. Therefore, we did not include the smooth adsorption site isomer. For both of the interesting isomers we have then performed a local geometry optimization as described in Sec. IV. We emphasize that the HI librational wavefunction is diagonalized in each step of the optimization. The HI dopant is slightly too large to perfectly fit into a substitutional position in the argon cluster, but at the same time the interaction energy between HI and argon atom is larger than that between two argon atoms. As a consequence of these contradicting tendencies, the argon cage relaxes and the argon-argon distances increase. The HI dopant in the surface is, compared to argon, slightly more extending into free space, but still remains an integral part of the third argon layer.

For a correct description of the HX-Rg_n photodissociation dynamics the HX librational wavefunction ϕ_{lib} is the key component of the vibrational wavefunction. If the hydrogen halide molecule is embedded in the cluster, we observe an almost free rotation of HI. This is a consequence of the high symmetry of this solvation site and the short range character of the van der Waals forces. The pronounced asymmetry of the surrounding argon atom arrangement leads to a strong orientation of HI molecules in the surface embedded position. It is not trivial to describe the orientation of the HI molecule on the surface of an argon cluster in a suitable way. The interaction potential between HI and argon shows two collinear minima. The lower minimum corresponds to the H-I...Ar arrangement while the secondary minimum has hydrogen pointing towards the argon atom (I-H...Ar). The first minimum is energetically preferred by approximately 50 cm^{-1}. After accounting for zero point motions, the ground state energies D_0 differ, however, by only 8 cm^{-1}.[34] Thus, for the HI-Ar system the hydrogen wavefunction is oriented away from the argon atom. If this were also the case for larger argon clusters, no appreciable caging should be observed for the surface isomer. We have addressed the question of the hydrogen orientation in our previous study[12] and we found a flip of the hydrogen wavefunction towards the argons while going from the HI-Ar_2 to the HI-Ar_3 cluster. We observed a back-flip for HI-Ar_4 (with a librational wavefunction pointing outside of the cluster once again). However, HI-Ar_5 and all larger clusters had hydrogen consistently pointing towards the argon cluster. It is important to emphasize that quantum delocalization (i.e., the zero point energy) plays a major role in the determination of the distribution of hydrogen orientations. All our calculations in Ref. 12 for larger clusters have been performed with an approximate wavefunction (see Eq. 3). Since quantum effects are so important in this case, we have decided to re-calculate the ground state wavefunctions for these clusters with the Diffusion Monte Carlo Method. This method provides in principle the fully coupled ground state wavefunction. The composite Fig. 9 depicts for HI-Ar_n(n=1-6) the projection of the square of the wavefunction as a function of cosΘ, where Θ is the angle between the HI molecular axis and the vector connecting the argon cluster center of mass with HI center of mass. The librational wavefunction corresponds to hydrogen pointing away from the rare gas atoms for HI-Ar and HI-Ar_2 clusters. Beginning with HI-Ar_3, the hydrogen atom is oriented towards the argon cluster. Unlike for reduced dimensionality calculations, the change is gradual and there is still some probability to find the hydrogen atom pointing away from the cluster for HI-Ar_3. No back-flip at HI-Ar_4 is observed. We conclude that the general trend of the change of the hydrogen orientation has been confirmed by the DMC calculations, while the back-flip for HI-Ar_4 has been found to be an artefact of the previous approximate vibrational calculations. The implications of the size evolution of the librational wavefunction on the photodissociation dynamics are discussed in the next section.

C. Photodissociation dynamics

In this section we discuss the results of molecular dynamics simulations of a HI molecule in/on argon clusters. When a bare HI molecule is irradiated by 243 nm light, three excited states are populated: the $^3\Pi_1$ and $^1\Pi_1$ states corresponding to H+I asymptote and the $^3\Pi_{0+}$ state, which correlates with the H+I* asymptote. Since hydrogen atoms promoted to the $^3\Pi_1$ and $^1\Pi_1$ states acquire roughly the same excess energy, we will refer only to two states differing in their asymptote: the lower and the upper spin orbit state. All physical quantities for the lower spin orbit state are given as a combination for the $^3\Pi_1$ and $^1\Pi_1$ states. We assume that the branching ratios between these two states in the cluster are roughly the same as for the bare HI molecule.[21,49]

A quantity that is readily available from the experiment is the kinetic energy distribution of hydrogens leaving the cluster (the KED spectrum). The results are presented in Fig. 6 for the different states. The upper part displays the quantity $P_e(E)$ which is reached by polarization 0°, while the lower part displays $P_g(E)$ which is reached by 90° polarization. The grey line represents the KED spectrum for the surface isomer, while the black line shows the same quantity for the HI molecule placed in the second solvation shell. The difference between the lower and upper spin-orbit state is basically only in the excess energy which is available to the hydrogen fragment. While the excess energy for the lower state is about 2 eV, the excess energy for the upper spin-orbit state is roughly 1 eV. The intensities in the KED around 2 eV and around 1 eV, therefore, provide information about the fraction of hydrogens freely exiting the cluster. Both for the surface and the second shell isomers and for both spin-orbit asymptotes we see that even though a certain fraction of hydrogens is slowed down, a significant part of the hydrogen atoms escapes freely. Let us first concentrate on clusters with the HI impurity placed in the second shell. In this case, the peak near zero kinetic energy corresponding to trapped and slowed down hydrogen fragments is more pronounced for the H+I* channel (Fig. 6a) than for the H+I state (Fig. 6b). This observation can be easily rationalized: the molecule is basically inside the cluster and when it is promoted to the $^3\Pi_{0^+}$ state it does not have enough energy to escape from the cluster. When we excite to the $^3\Pi_1$ or $^1\Pi_1$ states, the more energetic hydrogens have a better chance to escape. The situation is reversed for the surface isomer. In that case, the hydrogen atom is pointing towards the cluster. The fast component of the KED spectrum is formed by those hydrogens which are directly reflected from the surface of the argon cluster. The faster the hydrogen, the larger is its probability to penetrate into the cluster and to slow down. As a result, the fast peak in the KED spectrum is more pronounced for the surface isomer in the H+I* asymptote, while the opposite is true for the second shell isomer.

Let us return to the question why do we observe significant caging in the HI-Ar$_n$ photodissociation experiment and in the simulations at all. As we already discussed in the previous section, the small HI-Ar has a structure with the hydrogen pointing away from the argon atom. This implies that no cage effect should be observed in the photodissociation of the HI-Ar complex. Indeed, no low energy signal in the KED spectrum has been observed for this system[24], while for the similar Ar-HBr cluster, which has a hydrogen between the heavy atoms, a weak single atom cage effect has been observed.[54] The fact that we observe an important fraction of slow hydrogens for large clusters can indicate that either the pick-up procedure does not prepare the surface isomer or that the hydrogen wavefunction flips towards the argon cluster in response to an increase of the cluster size. We have shown above that the latter is an explanation, and we exclude the former hypothesis below.

A more detailed view at the difference between the photodissociation of HI on the surface and in the second solvation shell is provided by plotting the angular distribution of photodissociated hydrogen atoms. In Fig. 10 the plots of hydrogen atom populations with a given energy scattered by an angle Θ_D from the initial HI orientation are displayed. For the lower (upper) spin-orbit asymptote this quantity is denoted as $P_g(\Theta_D, E)$ ($P_e(\Theta_D, E)$). We can conclude that the fast hydrogens are not scattered significantly for the second shell isomer. This is because they would loose energy during scattering and remain within the cluster. The distribution of slow hydrogen atoms also peaks at small scattering angles with an almost isotropic background (i.e., having a $\sin\Theta_D$ dependence). Slow hydrogen atoms undergo many collisions, therefore, they loose all memory of the initial orientation. The picture for the surface isomer is very different. Fast hydrogens are strongly scattered. The reason is that hydrogens which do not change their initial direction penetrate into the cluster where they are slowed down. It is also interesting that even the slow hydrogen atoms are not isotropically distributed, although the distribution is broader than for the highly energetic hydrogen atoms. The explanation lies in the strong orientation of HI at the surface. It is very unlikely to observe a hydrogen atom which left the cluster with a zero scattering angle since this would mean that this hydrogen has penetrated through the whole cluster. For the Ar_{147} cluster this effectively means to pass through six solvation layers. Thus, slow hydrogen can escape from the cluster primarily sideways or in the backward direction.

VI. COMPARISON WITH EXPERIMENT

For a bare hydrogen iodide molecule, the experimental setup allows us to distinguish between hydrogen atoms originating from the two spin-orbit states. The apparatus set to 0° polarization registers hydrogens coming from the upper channel, while at 90° polarization it counts only hydrogens coming from the lower spin-orbit asymptote. This simple picture of the experimental results is completely lost, when HI is placed on or in an argon cluster (see Fig. 6). The calculation of the photodissociation events only adds correctly the cage effect at zero energy transfer, but fails to account for the contributions from the direct cage exits caused by the non-excited state. The reason for these contributions in the experiment must have a different origin. As was discussed in detail in the preceeding section, the scattering of dissociating hydrogens is the source of these contributions from the non-excited states. The measured kinetic energy distribution spectrum is then a function of the two-dimensional distributions $P_g(\Theta_D, E)$ and $P_e(\Theta_D, E)$. Measurements have been made with two laser polarizations, either 0° or 90°, i.e., parallel or perpendicular to the detector axis.

Figures 11 and 12 present experimental KED spectra for the two polarizations, together with the results of molecular dynamics simulations. MD histograms were obtained by processing the two-dimensional distribution functions $P_g(\Theta_D, E)$ and $P_e(\Theta_D, E)$ according to Eq. 7. Figure 11 shows the comparison for the surface isomer. The agreement between the simulation and the experiment is excellent for both polarizations. Although there is more intensity around 2 eV for the 90° polarization than for the 0° experiment, the difference is not very pronounced. This indicates that hydrogen atom scattering from the cage plays a crucial role in this process. The agreement between the theoretical calculation and the experiment for the second solvation shell isomer (Fig. 12) is still very good for the 0° polarization experiment, since the simulation results for both isomers do not differ very much for this polarization. This is surprising since the KED spectra for these two cluster isomers are different for the lower and upper asymptote (see Fig. 6). Clearly, the hydrogen atom scattering diminishes the differences. There is, however, a clear disagreement between simulation and experiment for the 90° polarization photodissociation of HI placed in the second shell position. The experimental fast component of the lower state (around 2 eV) is in this case significantly lower than the theoretical estimate, while that of the upper state is higher. Comparison of photodissociation simulations with the polarized light experiment thus indicates that HI lands in the surface and not in the second argon layer. This result is also in agreement with the results of the pick-up simulations.

VII. DISCUSSION AND CONCLUSION

We have measured the kinetic energy distribution of the H atom products after the photodissociation of HI molecules which are generated on the surface of an Ar_{139} cluster. Using polarized laser light at 243 nm the resulting distributions are dominated by peaks at 0.0, 1.0, and 2.0 eV. These values correspond to complete caging and unperturbed cage exits into the excited H+I* and the ground H+I spin orbit states. In contrast to the results for the bare molecule, where the excited spin-orbit state is reached by a pure parallel and the ground spin-orbit state by a pure perpendicular transition, the intensities in the cluster are completely scrambled. This is, of course, expected for the caged H atoms, but a bit unusual for the cage exit case. To clarify the situation a series of calculations have been carried out using MD simulations to model the landing of HI on the cluster and mixed quantum-classical calculations for the dissociation process. The results are as follows. (i) The HI dopant lands in a substitutional surface position of the large argon cluster. To obtain this result the accurate Ar-Ar interaction potential of Aziz and coworkers has to be used. (ii) The very existence of the cage effect which is not observed for small systems is traced back to a gradual flip of the HI librational wavefunction with increasing cluster size. (iii) The scrambling of the intensities resulting from the perpendicular and the parallel transitions is explained by accounting for the scattering of the H atom within the cluster. Inclusion of all three effects gives very nice agreement between the measured and calculated kinetic energy distributions. The initial position of the HI molecule in the second shell could be ruled out both by the simulation of the landing process and the comparison of the calculated results with the measurements. In addition, it turned out not to be necessary to invoke any change in the branching ratio caused by the presence of the rare gas environment.

We note that there are two other possibilities that could be responsible for the intensity mixing. The first one is a cluster induced change of the transition moment. Such an effect should depend on the interaction with the rare gas host and increase for larger masses. The second effect is caused by non-adiabatic interactions in the final channel potentials which would also lead to a redistribution of the intensities. In principle, we cannot distinguish experimentally between these two scenarios and the scattering processes. The fact, however, that already the inclusion of the obvious scattering effects explain completely the experimental results is a convincing hint that the other two effects play only a minor role.

Interestingly, there also exist some experimental proofs to test this. As mentioned above the change of the transition moment should strongly depend on the rare gas. We observe, however, for HI-Kr_n and HI-Xe_n about the same kinetic energy distributions as for the present system.[23] In addition, there is the possibility to test the second assumption, the final state interaction, by changing the dissociation wavelength to 193 nm. At this energy the absorption due to the $^3\Pi_{0+}$ and the $^3\Pi_1$ state dies out so that only the excitation of the $^1\Pi_1$ state is left. This is a pure perpendicular transition which leads always to the ground spin-orbit state. Note, that any measured intensity in the excited state at this wavelength would be an indication of the final state non-adiabatic interaction.

If we compare the results for HI-Ar_n with those of the other two measured hydrogen halides, HCl-Ar_n[28] and HBr-Ar_n[22], it is obvious that due to the large spin-orbit coupling this is the only system where we observe the possibility of a perpendicular and a parallel transition with about the same probability. This is, in fact, the reason for the observed unusual behavior. In the case of HCl-Ar$_n$ the spin-orbit coupling is small and the excitation proceeds only by a perpendicular transition. The molecule is deeply buried in a perfect substitutional position in the surface and thus nearly no cage exit is observed. The HBr-Ar$_n$ system, is an intermediate case. The molecule is sitting in a slightly disturbed, substitutional surface position, so that cage exit processes ican occur. At 193 nm it behaves similar to HCl with a dominating perpendicular transition. At 243 nm we find a perpendicular transition to the ground state and a parallel transition to the excited state similar to the behavior of HI. The branching ratio, however, is only 0.20 so that the pronounced mixing of the states by scattering as was observed for HI is much weaker. Thus, HI-Ar$_n$ is up to now the only system with such a drastic redistribution of intensity.

Acknowledgment

Support of the Czech Ministry of Education to the Center for Complex Molecular Systems and Biomolecules (Grant No. LN00A032) is gratefully acknowledged. The work in Göttingen was supported by the Deutsche Forschungsgemeinschaft in Sonderforschungsbereich 357. M.F. gratefully acknowledges the support of the Alexander von Humboldt Foundation.

[1] R. B. Gerber, A. B. McCoy, and A. García-Vela, Ann. Rev. Phys. Chem. **45**, 275 (1994).

[2] U. Buck, J. Phys. Chem. A **106**, 10049 (2002).

[3] R. Alimi and R. B. Gerber, Phys. Rev. Lett. **64**, 1453 (1990).

[4] T. Schröder, R. Schinke, S. Liu, Z. Bačić, and J. W. Moskowitz, J. Chem. Phys. **103**, 9228 (1995).

[5] M. Niv, A. I. Krylov, and R. B. Gerber, Faraday Discuss. Chem. Soc. **108**, 243 (1997).

[6] M. Y. Niv, A. I. Krylov, R. B. Gerber, and U. Buck, J. Chem. Phys. **110**, 11047 (1999).

[7] P. Žďánská, B. Schmidt, and P. Jungwirth, J. Chem. Phys. **110**, 6246 (1999).

[8] B. Schmidt, Chem. Phys. Lett. **301**, 207 (1999).

[9] P. Žďánská, P. Slavíček, and P. Jungwirth, J. Chem. Phys. **112**, 10761 (2000).

[10] R. Baumfalk, N. H. Nahler, U. Buck, M. Y. Niv, and R. B. Gerber, J. Chem. Phys. **113**, 329 (2000).

[11] P. Slavíček, P. Žďánská, P. Jungwirth, R. Baumfalk, and U. Buck, J. Phys. Chem. A **104**, 7793 (2000).

[12] P. Slavíček, M. Roeselová, P. Jungwirth, and B. Schmidt, J. Chem. Phys. **114**, 1539 (2001).

[13] M. Monnerville and B. Pouilly, Chem. Phys. Lett. **294**, 473 (1998).

[14] J. Trin, M. Monnerville, B. Pouilly, and H. D. Meyer, J. Chem. Phys. **118**, 600 (2003).

[15] B. Lepetit and D. Lemoine, J. Chem. Phys. **117**, 8676 (2002).

[16] R. Prosmiti and A. Garcia-Vela, J. Chem. Phys. **117**, 100 (2002).

[17] A. García-Vela, J. Chem. Phys. **108**, 5755 (1998).

[18] E. Narevicius and N. Moiseyev, Chem. Phys. Lett. **287**, 250 (1998).

[19] H. M. Lambert, P. J. Dagdigian, and M. H. Alexander, J. Chem. Phys. **108**, 4460 (1998).

[20] G. Peoux, M. Monnerville, T. Duhoo, and B. Pouilly, J. Chem. Phys. **107**, 70 (1997).

[21] R. J. LeRoy, G. T. Kraemer, and S. Manzhos, J. Chem. Phys. **117**, 9353 (2002).

[22] N. H. Nahler, R. Baumfalk, U. Buck, H. Vach, P. Slavíček, and P. Jungwirth, Phys. Chem. Chem. Phys. **xxx**, submitted (2003).

[23] R. Baumfalk, N. H. Nahler, and U. Buck, Faraday Disscus. **118**, 247 (2001).

[24] C. Jaques, L.Valachovic, S. Ionov, E. Bömer, Y. Wen, J. Segall, and C. Wittig, J. Chem. Soc. Faraday Trans. **89**, 1419 (1993).

[25] T. Suzuki, H. Katayanagi, and M. C. Heaven, J. Phys. Chem. **101**, 6697 (1997).

[26] U. Buck, R. Galonska, H. J. Kim, P. Lohbrandt, C. Lauenstein, and M. Schmidt, in *Atomic and Molecular Beams. The State of the Art 2000*, edited by R. Campargue (Springer, Berlin, 2001), p. 623.

[27] R. Baumfalk, U. Buck, C. Frischkorn, S. R. Gandhi, and C. Lauenstein, Ber. Bunsenges. Phys. Chem. **101**, 606 (1997).

[28] N. H. Nahler, M. Farnik, U. Buck, H. Vach, M. Niv, and R. B. Gerber, J. Chem. Phys. p. in preparation (2003).

[29] O. F. Hagena, Surf. Sci. **106**, 101 (1981).

[30] S. Schütte and U. Buck, Intern J. Mass Spectr. **220**, 183 (2002).

[31] W. C. Wiley and I. H. McLaren, Rev. Sci. Instrum. **26**, 1150 (1955).

[32] R. Baumfalk, U. Buck, C. Frischkorn, N. H. Nahler, and L. Hüwel, J. Chem. Phys. **111**, 2595 (1999).

[33] S. R. Langford, P. M. Regan, A. J. Orr-Ewing, and M. N. R. Ashfold, Chem. Phys. **231**, 245 (1998).

[34] A. McIntosh, Z. Wang, J. Castillo-Chara, R. R. Lucchese, J. Bevan, R. D. Suenram, and A. C. Legon, J. Chem. Phys. **111**, 5764 (1999).

[35] R. A. Aziz and M. J. Slaman, Mol. Phys. **58**, 679 (1986).

[36] G. Herzberg, *Molecular Spectra and Molecular Structure* (Van Nostrand, New York, 1950).

[37] J. O. Hirschfelder, C. F. Curtiss, and R. B. Bird, *Molecular Theory of Gases and Liquids* (Wiley, New York, 1954).

[38] Y. X. Zhao, I. Yourshaw, G. Reiser, C. C. Arnold, and D. M. Neumark, J. Chem. Phys. **101**, 6538 (1994).

[39] G. Van Veen, K. Mohamed, T. Baller, and A. De Vries, Chem. Phys. **80**, 113 (1983).

[40] H. Vach, J. Chem. Phys. **113**, 1097 (2000).

[41] M. P. Allen and D. J. Tildesley, *Computer Simulations of Liquids* (Clarendon Press, Oxford, 1987).

[42] B. L. Hammond, W. A. Lester, Jr., and P. J. Reynolds, *Monte Carlo Methods in ab initio Quantum Chemistry* (World Scientific, Singapore, 1994).

[43] P. J. Reynolds, D. M. Ceperley, B. J. Alder, and W. A. Lester, Jr., J. Chem. Phys. **77**, 5593 (1982).

[44] C. J. Umrigar, M. P. Nightingale, and K. J. Runge, J. Chem. Phys. **99**, 2865 (1993).

[45] M. Lewerenz, J. Chem. Phys. **104**, 1028 (1996).

[46] D. Blume, M. Lewerenz, F. Huisken, and M. Kaloudis, J. Chem. Phys. **105**, 8666 (1996).

[47] B. M. Auer and A. B. McCoy, J. Phys. Chem. A **107**, 4 (2003).

[48] M. Hillery, R. F. O'Connel, M. O. Scully, and E. P. Wigner, Phys. Rep. **106**, 121 (1984).

[49] A. Alekseyev, H. P. Liebermann, D. Kokh, and R. Buenker, J. Chem. Phys. **113**, 6174 (2000).

[50] J. Farges, M. de Feraudy, B. Raoult, and G. Torchet, J. Chem. Phys. **84**, 3491 (1986).

[51] A. Michels, H. Wijker, and H. Wijker, Physica **15**, 627 (1949).

[52] J. A. Barker, in *Rare Gas Solids, Vol. 1*, edited by M. L. Klein and J. A. Venables (Academic Press, New York, 1976), p. 212.

[53] R. P. Feynman and A. R. Hibbs, *Quantum Mechanics and Path Integrals* (McGraw-Hill, New Yourk, 1965).

[54] J. Segall, Y. Wen, R. Singer, C. Wittig, A. García-Vela, and R. Gerber, Chem. Phys. Lett. **207**, 504 (1993).

FIG.1: Interaction potentials (upper part) and absorption coefficients (lower part) for the photodissociation of HI molecules. Data for both figures from Ref. 21.

FIG.2: Pictorial view of the experimental apparatus in the left part. The middle and right parts explain the geometric conditions in the WM-TOFMS. The laser beam propagates perpendicularly to the plane of the paper. White circles depict the iodine atoms, small grey or black circles represent hydrogen atoms, and tiny double-headed-arrows indicate the transition dipole moment of the HI molecules.

FIG.3: H atom TOF spectra from the photodissociation of pure HI molecules. The measurement is represented by circles. The solid lines correspond to the TOF spectra from the Monte-Carlo trajectory simulation program.

FIG.4: Two-dimensional view of scattering processes of the H atom at the cluster cage following the photodissociation of HI. The rings depict the cluster shells. Solid line trajectories lead to the detector while the dashed ones are leaving the WM-TOFMS.

FIG.5: Three-dimensional view of HI molecule positions on the surface of the cluster represented as a ball. All HI molecules have a transition dipole moment parallel to the laser polarization. The outgoing H atoms can be scattered onto or away from the detector by interactions with the cluster cage.

FIG.6: Photodissociation of HI-Ar_n clusters: Experimental results (black points) for two laser polarizations and calculations after photoexcitation into the indicated states. The black line corresponds to the dopant in the second shell and the grey line to the dopant on the surface.

FIG.7: Pick-up of HI on Ar_{130} cluster using Lennard-Jones Ar-Ar potential.[37] a) Density of dopant atoms (solid line) in comparison with the density of argon atoms (histogram). b) Distribution of number of nearest neighbors of the dopant atom.

FIG.8: Pick-up of HI on Ar_{130} cluster using Aziz Ar-Ar potential.[35] a) Density of dopant atoms (solid line) in comparison with the density of argon atoms (histogram). b) Distribution of number of nearest neighbors of the dopant atom.

FIG.9: Size dependence of the DMC calculated ground vibrational (librational) wavefunction for HI on Ar_n ($n = 1 - 6$, corresponding to labels a) to f)). Wavefunction is depicted as a function of $\cos\Theta$ where Θ is the angle between the cluster center of mass and the center of mass of the dopant. Note that the flip of the H wavefunction towards the rare gas clusters with increasing cluster size seen for the calculations in reduced dimensionality is no more observed. The drop towards $\cos\Theta = 1$ and -1 is due to the inclusion of the volume element in the definition of the probability.

FIG.10: Angular and kinetic energy distribution of the outgoing hydrogen atoms. Graphs a) and c) correspond to the H + I exit channel, while b) and d) correspond to the H + I* channel. In cases a) and b) the dopant is placed into the second shell, while in cases c) and d) the dopant is in the surface.

FIG.11: Simulation of the photodissociation of the dopant on the surface (histogram) compared with a pick-up photodissociation experiment (line with points and error bars).

FIG.12: Simulation of the photodissociation of the dopant in the second shell (histogram) compared with a pick-up photodissociation experiment (line with points and error bars).

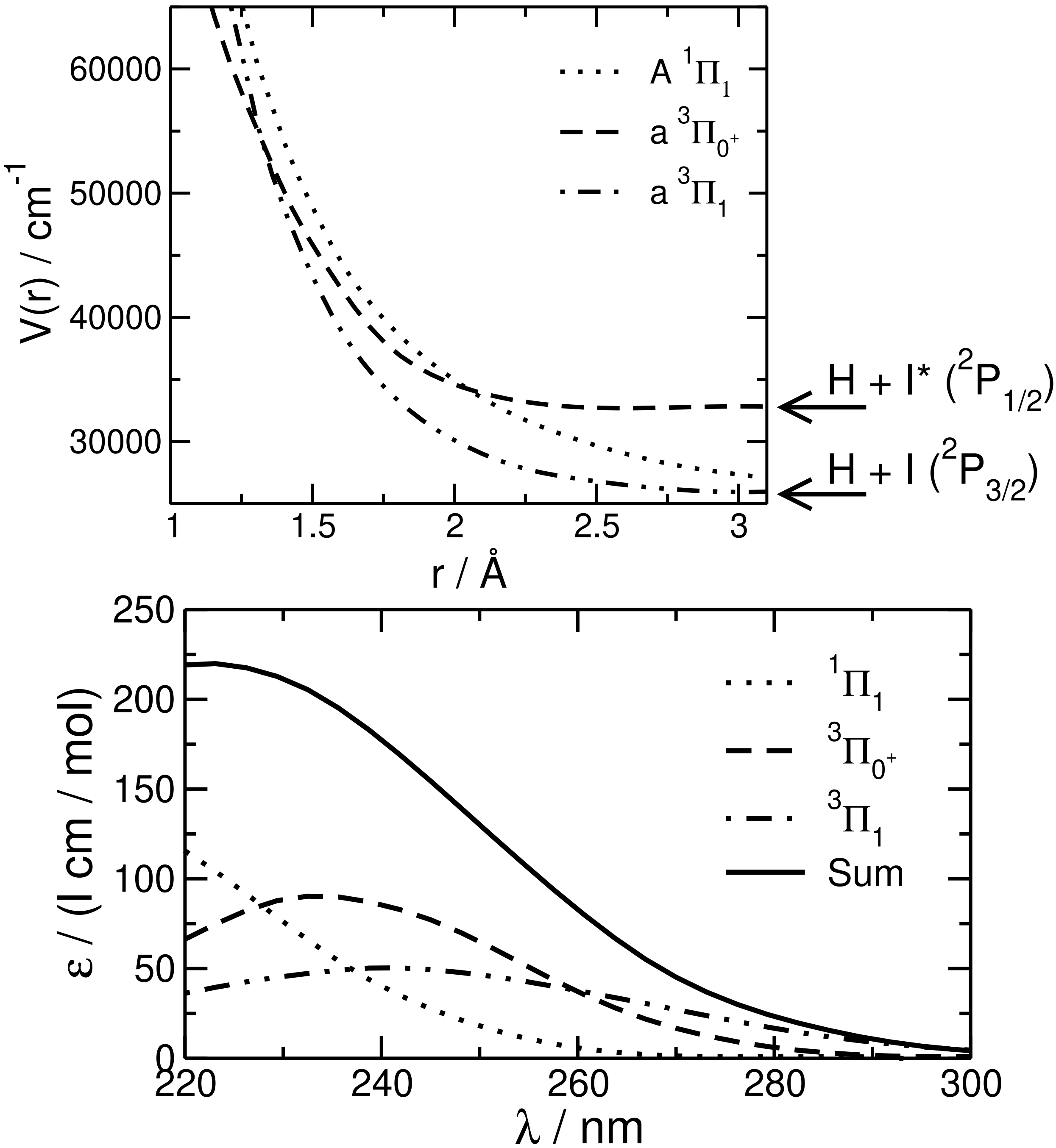

FIG. 1: Slavicek et al.

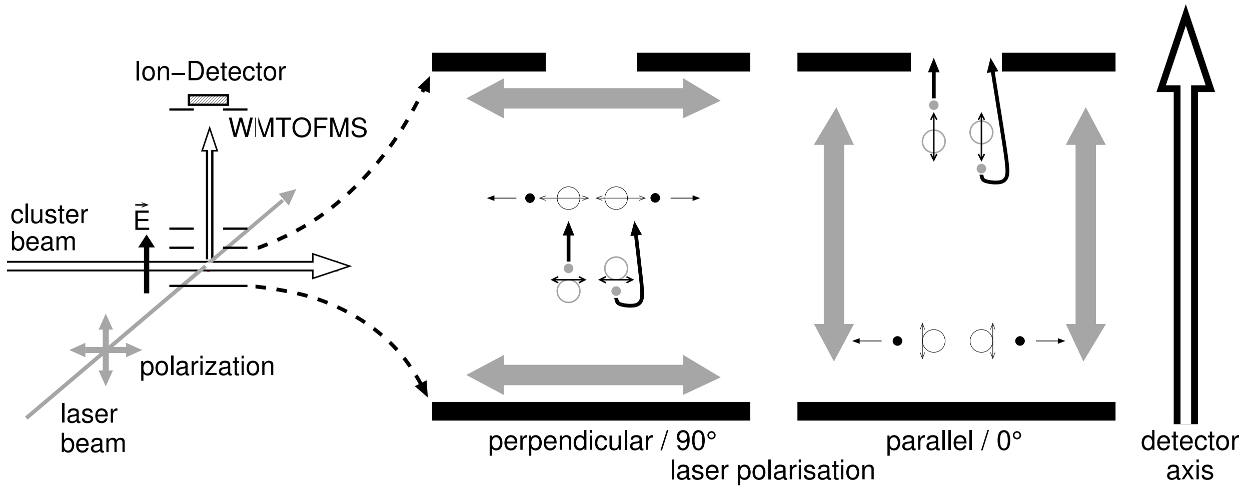

FIG. 2: Slavicek et al.

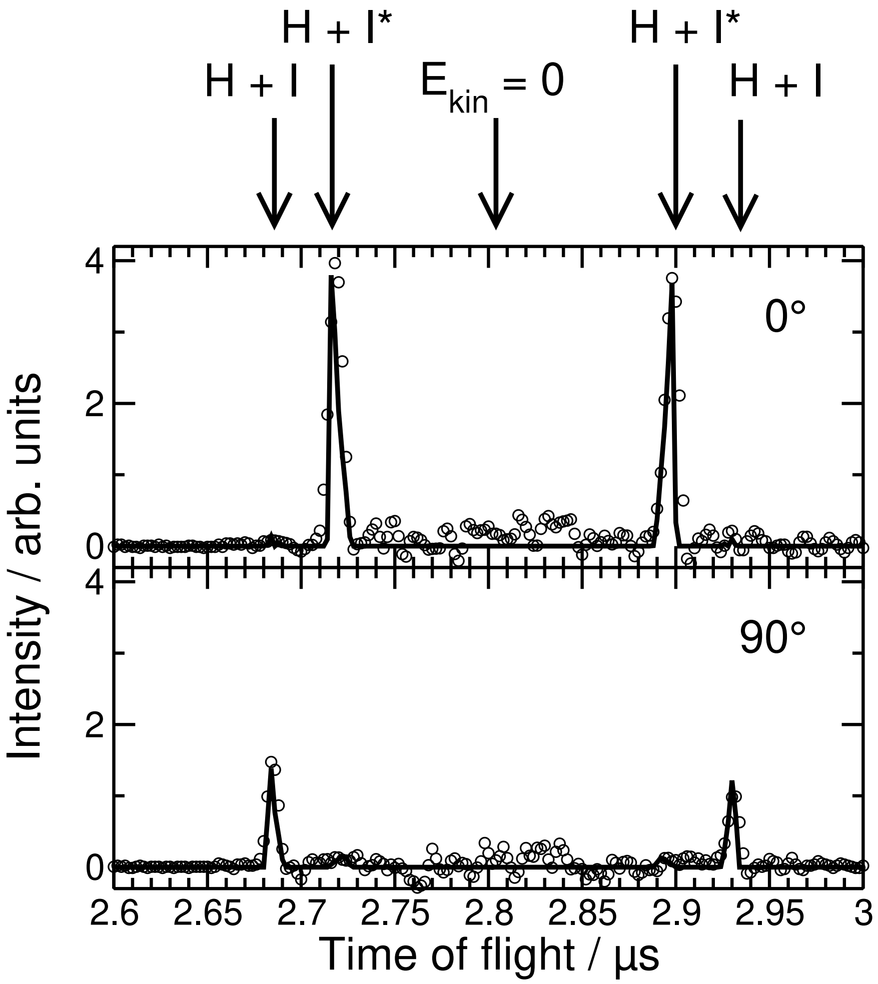

FIG. 3: Slavicek et al.

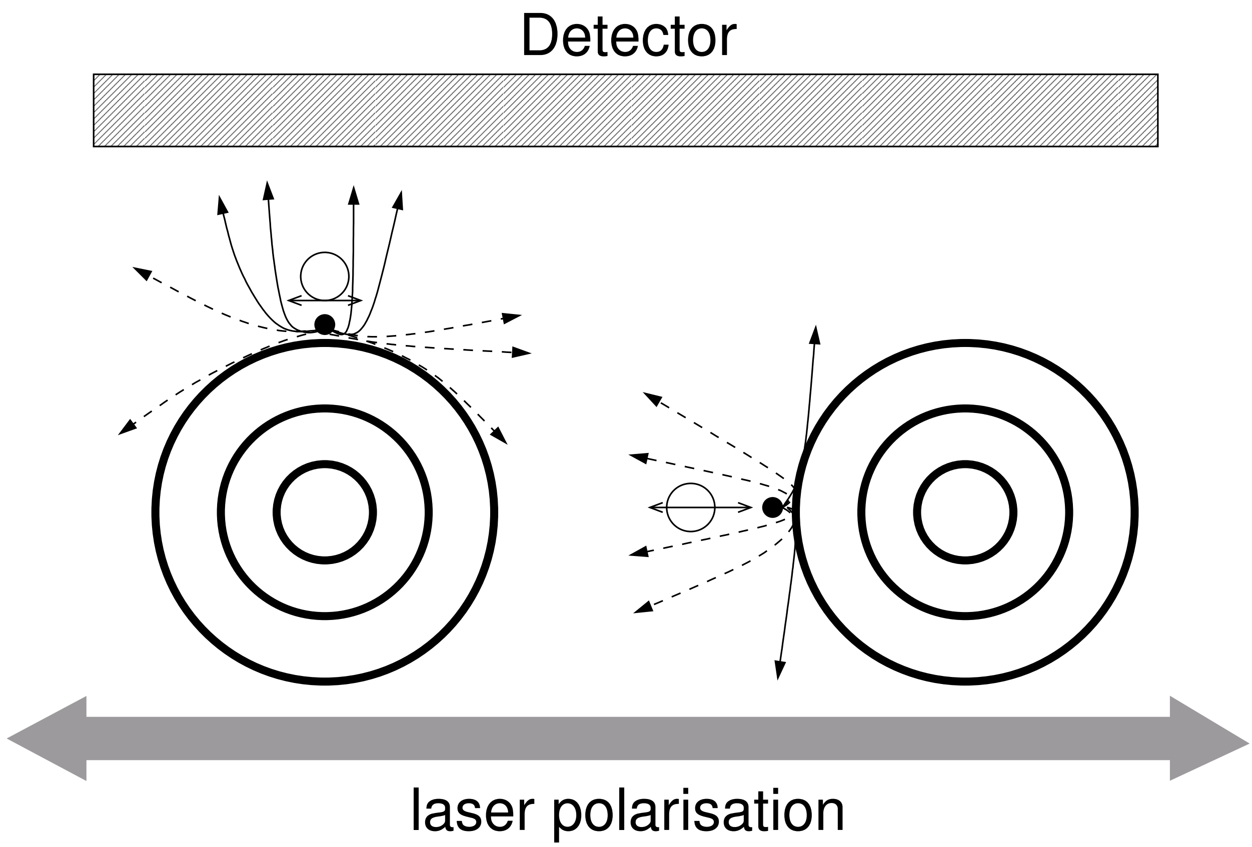

FIG. 4: Slavicek et al.

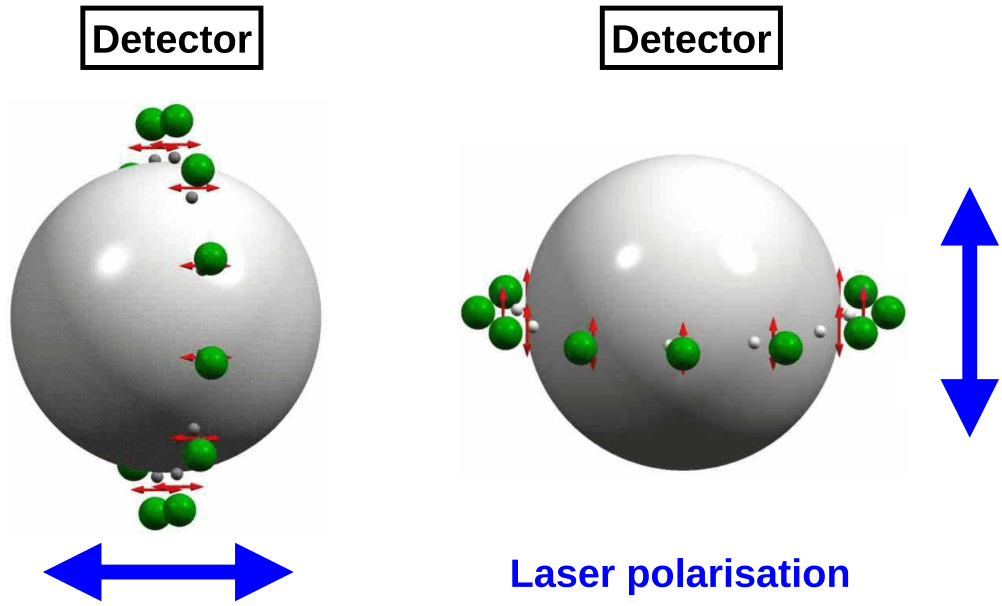

FIG. 5: Slavicek et al.

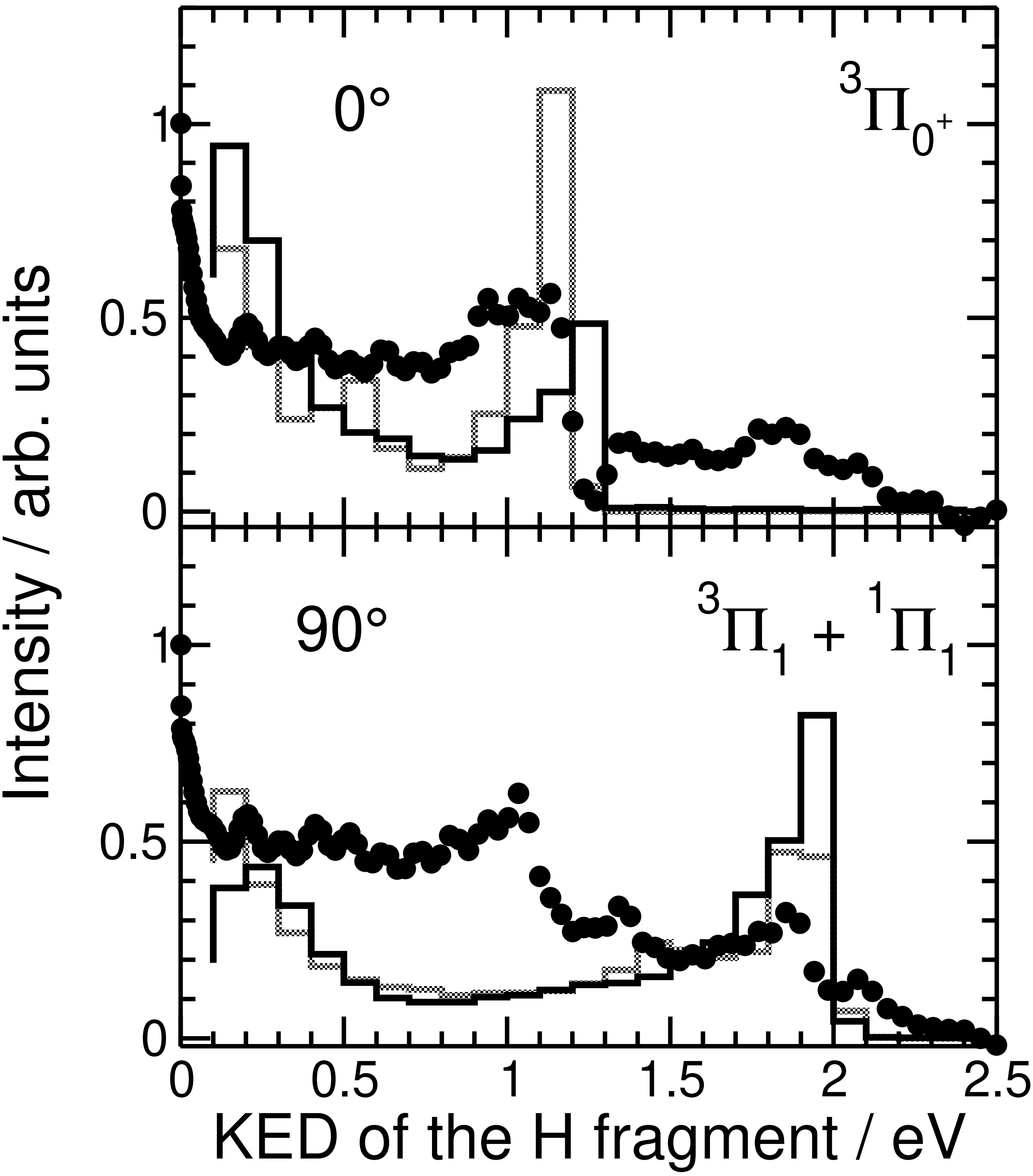

FIG. 6: Slavicek et al.

(a)

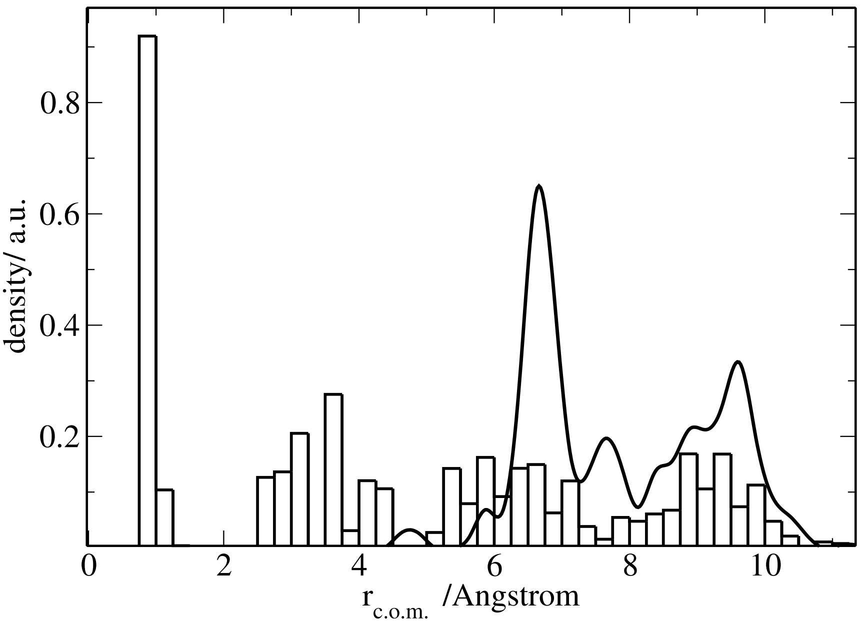

(b)

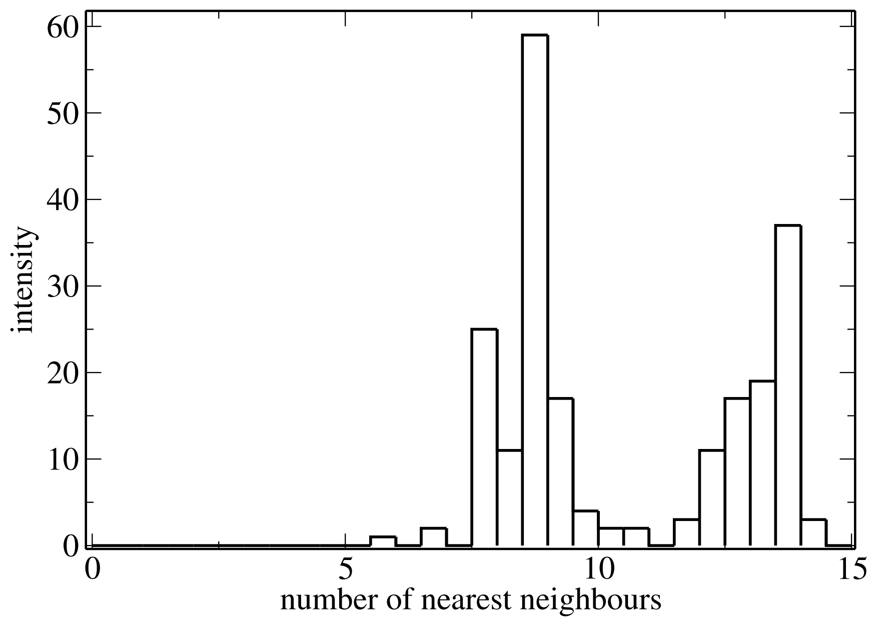

FIG. 7: Slavicek et al.

(a)

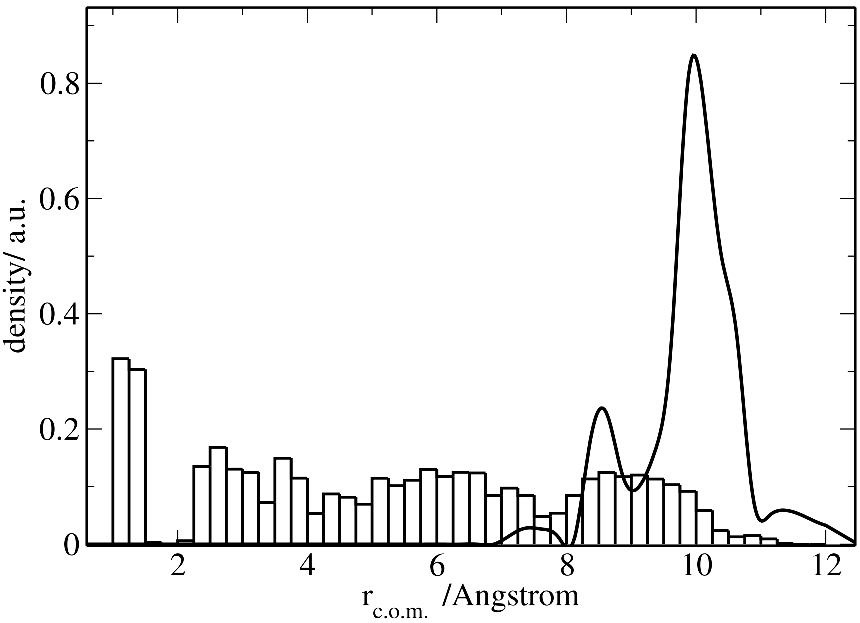

(b)

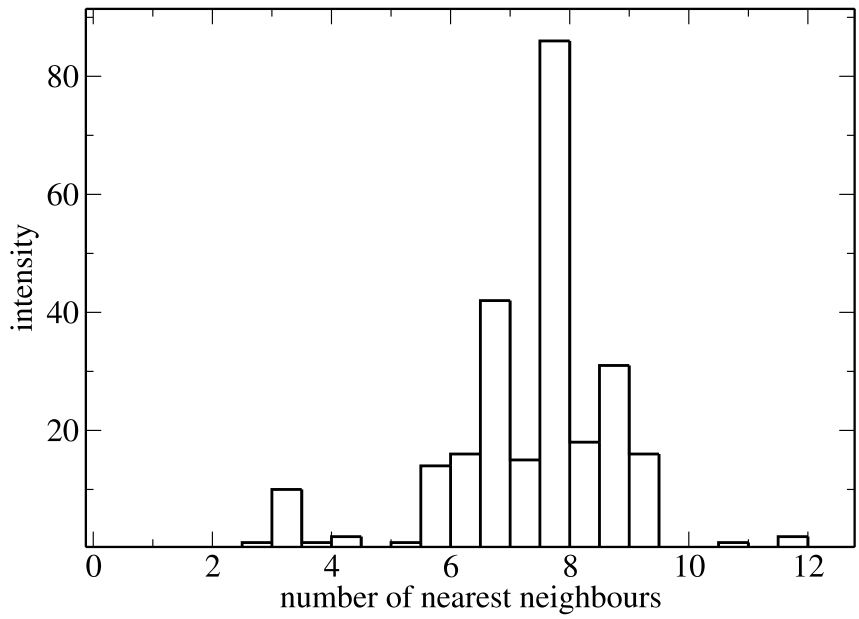

FIG. 8: Slavicek et al.

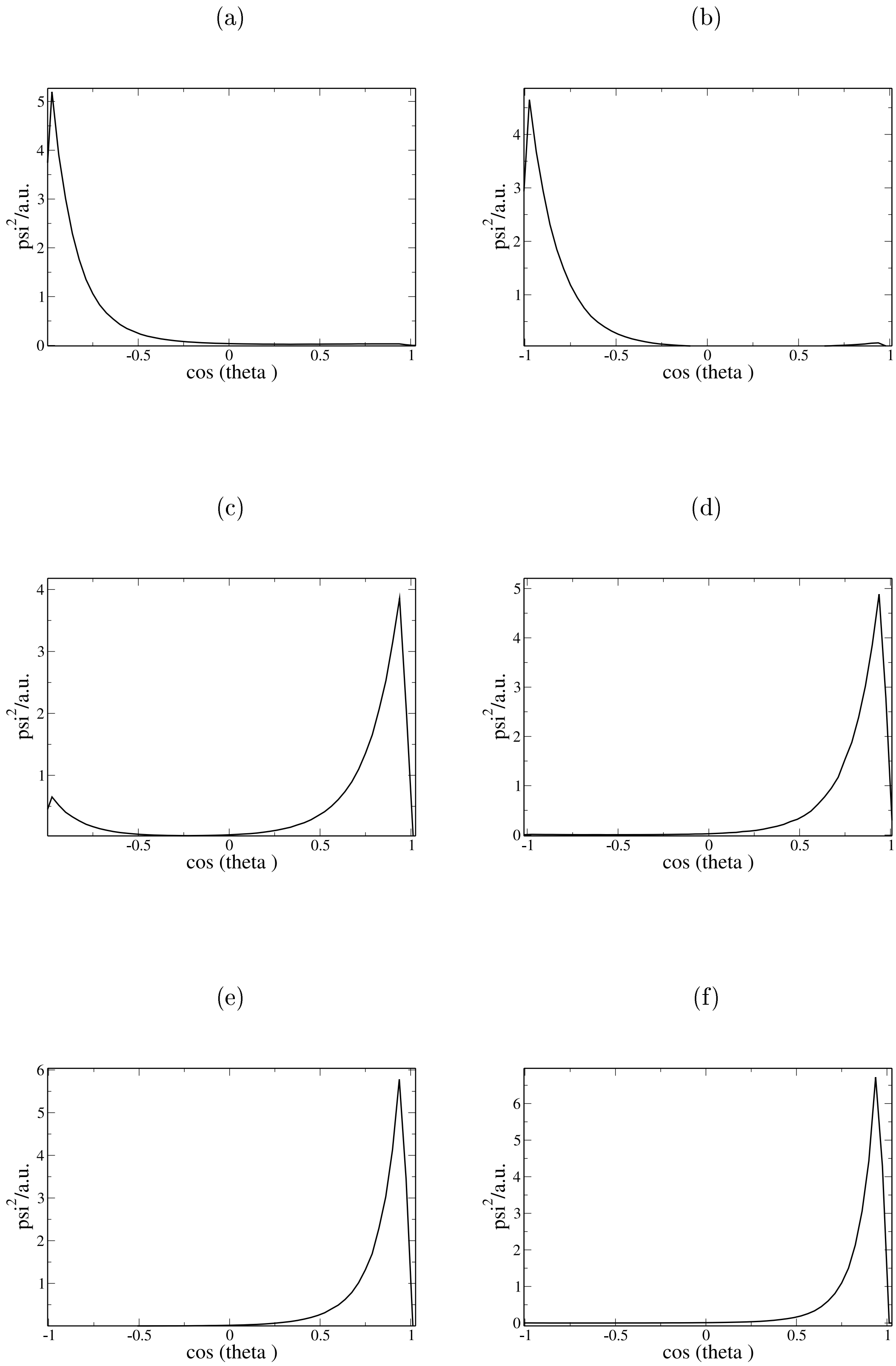

FIG. 9: Slavicek et al.

(a)

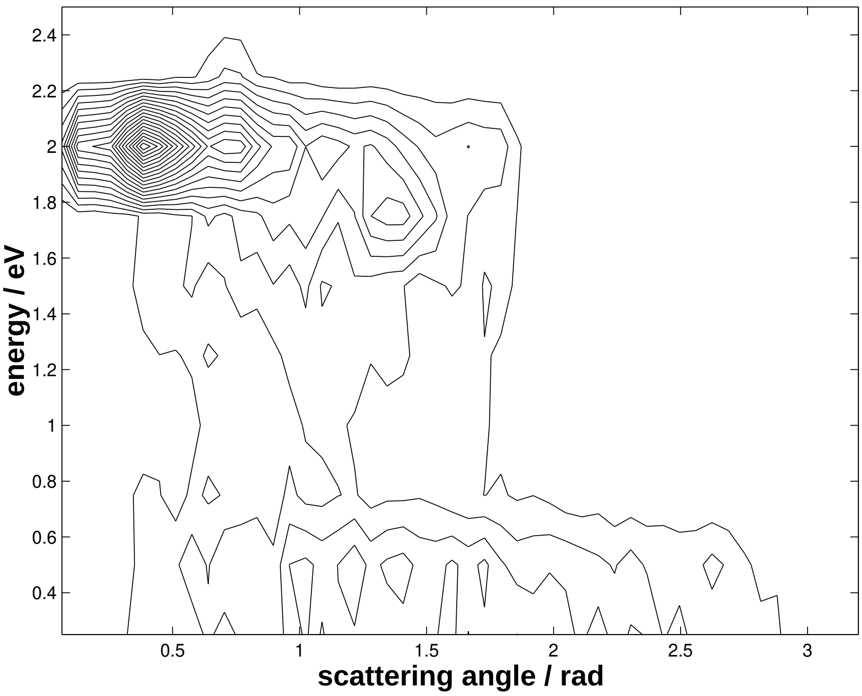

energy / eV
2.4
2.2
2
1.8
1.6
1.4
1.2
1
0.8
0.6
0.4
0.5
1
1.5
2
2.5
3
scattering angle / rad

(b)

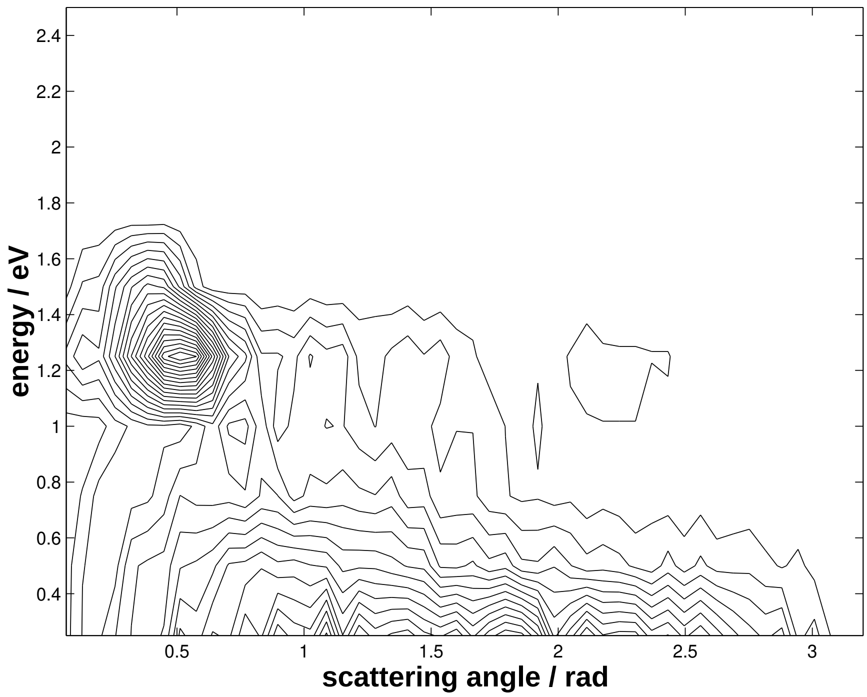

energy / eV
2.4
2.2
2
1.8
1.6
1.4
1.2
1
0.8
0.6
0.4
0.5
1
1.5
2
2.5
3
scattering angle / rad

(c)

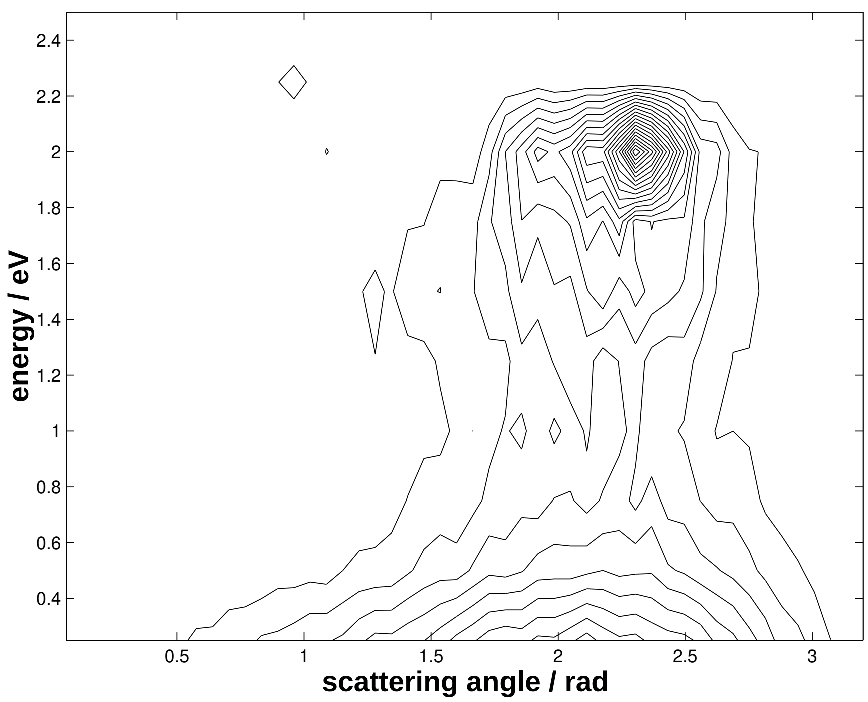

(d)

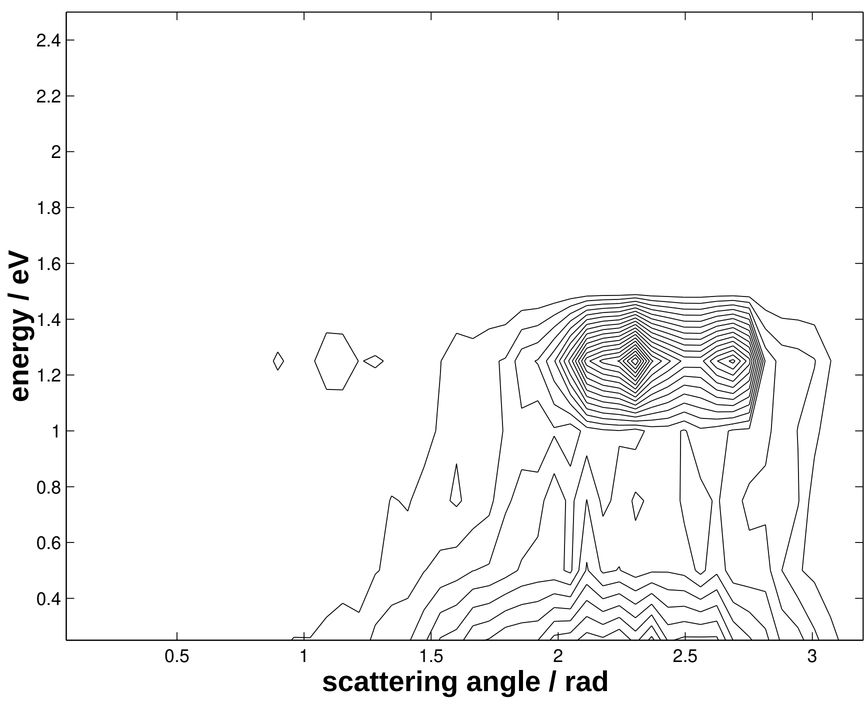

FIG. 10: Slavicek et al.

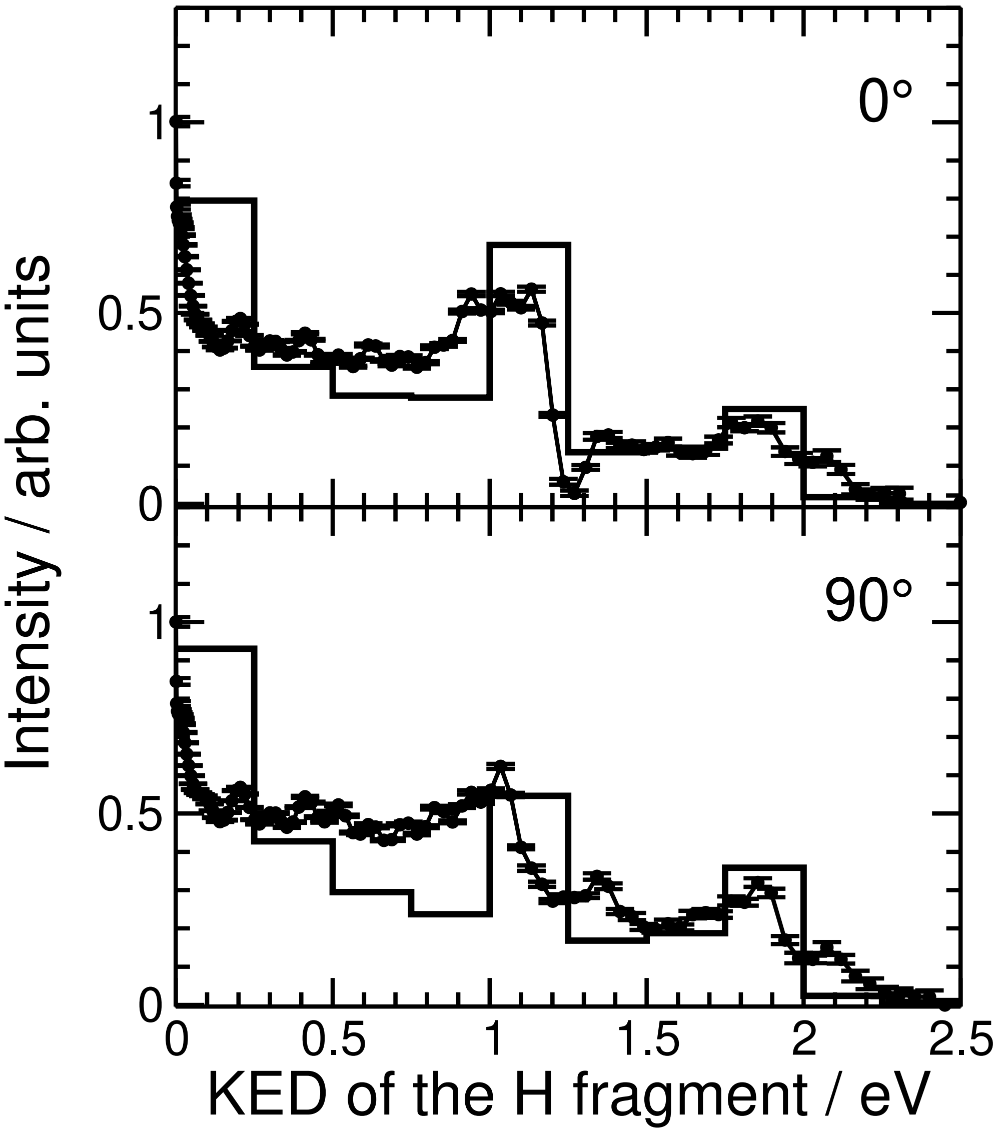

FIG. 11: Slavicek et al.

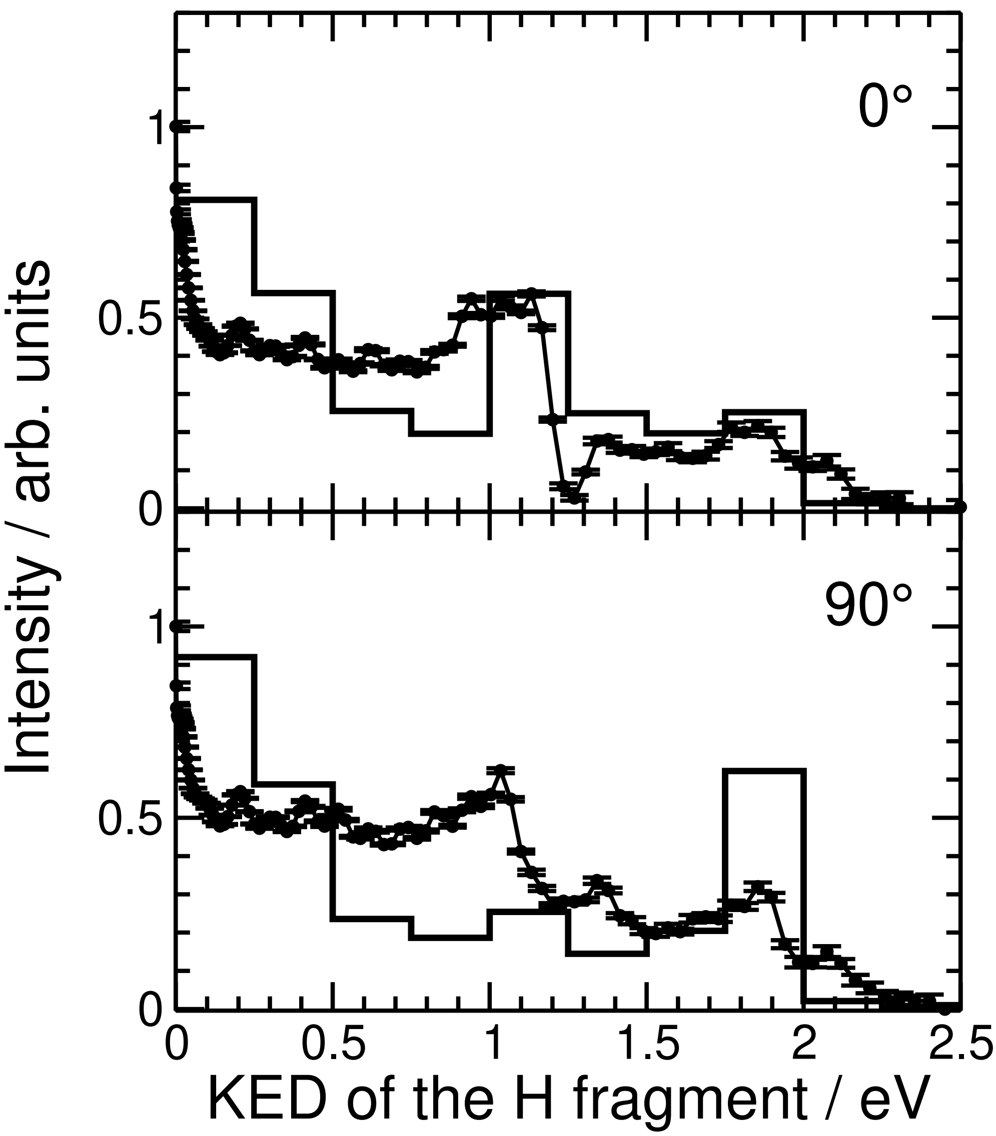

FIG. 12: Slavicek et al.